

## Variation in stress with background pressure in sputtered Mo/Si multilayer films

D. L. Windt, W. L. Brown, C. A. Volkert, and W. K. Waskiewicz

AT&T Bell Laboratories, 600 Mountain Ave, Murray Hill, NJ 07974

908-582-2367 \* 908-582-4228 Fax \* windt@physics.att.com

### ABSTRACT

We have measured the stress in Mo/Si multilayer films deposited by magnetron sputtering, using the wafer-curvature technique, and find a strong dependence on background pressure. We find that for multilayers containing 40 bilayers of  $\sim 4.3$  nm Si layers and  $\sim 2.6$  nm Mo layers, the stress increases from approximately  $-280$  MPa (compressive) to  $-450$  MPa as the background pressure in the deposition chamber (i.e., measured just prior to deposition) decreases from  $1.0 \times 10^{-5}$  to  $6.0 \times 10^{-8}$  torr. For multilayers of the same period but with thicker Mo layers, the dependence on background pressure is even stronger. X-ray ( $\lambda = 0.154$  nm) diffraction measurements reveal only a slight increase in interfacial roughness for films deposited at high background pressure, but no evidence was found for any differences in the microstructure of the polycrystalline Mo layers that comprise these structures. The peak soft X-ray ( $\lambda = 13$  nm) reflectance, which is sensitive to interfacial roughness at longer spatial wavelengths, also shows no correlation with background pressure or stress. Atomic concentrations of incorporated oxygen and carbon, measured with Auger electron spectroscopy, were found to be less than  $\sim 0.5$  at.% for all samples. However, the average hydrogen concentration, as determined from forward-recoil-scattering measurements made using a 2.6 MeV He beam, was found to vary from  $\sim 0.3$  at.% to  $\sim 1.6$  at.%, increasing with both background pressure and Mo layer thickness. We discuss possible mechanisms for the observed dependence of film stress on background pressure, including gas incorporation and the affect of residual gas atoms on adatom mobility.

## 1. INTRODUCTION

Periodic thin-film multilayer (ML) structures are interesting subjects for the study of film growth and interface formation [1, 2]. MLs are also being used for a variety of technological applications which take advantage of their unique optical, magnetic, electrical, and/or mechanical properties [3-7]. For many of these applications, the film stress is an important parameter that must be characterized and ultimately controlled. For instance, stress affects the adhesion of the film to the substrate, and also causes the substrate to deform, which may be of critical importance for certain applications, e.g., diffraction-limited X-ray imaging using reflective ML coatings, for which the surface figure of the ML-coated optics must be controlled to  $\sim 1$  nm [3]. Excessive stress will further limit our ability to produce flat, free-standing thin film MLs, as for X-ray beamsplitters, for example.

The stress in a ML film is determined by the stresses in the individual layers that comprise the ML, and by any interfacial stresses that may be present. The deposition stresses in the individual layers, i.e., the stresses resulting from non-equilibrium growth conditions, are highly dependent on the details of the deposition conditions. Thus, the stress in a ML film, as in a single-layer film, is process dependent, in general. For example, it is by now well-known that the stress in single-layer films prepared by magnetron sputtering can be adjusted from tensile to compressive simply by decreasing the pressure of the working gas [8], and the same effect was reported recently for ML films [9]. In order to control precisely the stress in ML films, we must, therefore, first characterize any dependencies of ML stress on deposition conditions.

In this paper we report the results of an investigation of the stress dependence on background pressure in ML films composed of molybdenum and silicon layers prepared by magnetron sputtering. The stress in Mo/Si MLs has been reported previously [10]. However, the dependence on stress with background pressure in these, or in any other ML structures has not, to our knowledge, been reported previously.

Previous investigations have shown that the highest quality Mo/Si MLs (i.e., those having well-defined layers with the smoothest interfaces, and consequently the highest peak soft X-ray reflectance) are

prepared by ion-beam sputtering or by magnetron sputtering at low Ar pressure [11]. Using both X-ray diffraction and transmission electron microscopy, MLs prepared under these conditions are known to be composed of amorphous Si layers and polycrystalline Mo layers, separated by amorphous interlayer regions of mixed composition. The bcc Mo crystallites show a preferred {110} orientation, which places the most densely populated planes parallel to the substrate. The interfacial roughness in these structures is small, nominally 0.1-0.2 nm; the predominant interface imperfection is the diffuseness associated with the interlayers.

## 2. BACKGROUND

Before we describe the experimental details and the results of our investigation, which we present in sections 3 and 4, respectively, it will be useful to review briefly the subject of thin film stress, with particular emphasis on the current understanding of the origins of deposition stresses in sputtered films. This background material will also aid in our analysis of the data, and in the discussion of our results in section 5.

The total stress in a ML film results from the stresses in the individual layers that comprise the ML, and from any interfacial stresses that may be present. The interfacial stress  $f$  is equal to the work required to deform elastically by a unit strain a unit area of interface [12]. For the case of a periodic ML film consisting of alternating layers of materials A and B, having thicknesses  $d_A$  and  $d_B$ , and biaxial stresses  $\sigma_A$  and  $\sigma_B$ , respectively, the total biaxial stress  $\sigma_{ML}$  in the film is independent of the number of periods, and is given by [13]

$$(1) \quad \sigma_{ML} = (d_A \sigma_A + d_B \sigma_B + 2f)/(d_A + d_B).$$

Several assumptions are implicit in this expression, including (a) that the ML consists of many periods, so that one may neglect both the interfacial stress term associated with the film-substrate interface, and the surface stress term associated with the top layer, (b) that the layers are isotropic in the plane of the film, and (c) that the interfaces between the layers are sharp, i.e. there is no intermixing between the A and B layers,

so that the interfaces and thus the interfacial stresses are well-defined.

Direct measurements of the interfacial stresses in ML films have been reported by Ruud *et al* [13] for the case of Ag/Ni MLs, and by Bain *et al* [14] for Mo/Ni MLs. In the former case, where the mutual solubility of Ag and Ni is small, and the Ag-Ni interfaces sharp, the interfacial stress was found to be  $-2.27 \pm 0.67 \text{ J/m}^2$ . In the Mo/Ni system, on the other hand, where the mutual solubilities of Mo and Ni are substantial and the interfaces are likely diffuse, no evidence for interfacial stresses was found. A measurement of the interfacial stress in Mo/Si MLs has not, to our knowledge, been reported; considering that the interfaces in these structures show considerable diffuseness, and in light of the results for Ag/Ni and Mo/Ni MLs, interfacial stresses in the Mo/Si system may be absent. We thus adopt the simplest view and assume that the interfacial stress term in equation (1) may be neglected.

Stresses in the individual layers of the ML, as in the case of a single layer film, can arise by several different mechanisms [15]. Thermal stress will result from a difference  $\Delta\alpha$  in the thermal expansion coefficient of the film relative to the substrate, according to

$$(2) \quad \sigma_{\text{Thermal}} = Y_f \Delta\alpha (T_D - T_M)$$

(for the case of a single film on a substrate), where  $Y_f$  is the biaxial elastic modulus of the film, and  $T_D$  and  $T_M$  are the film deposition and stress measurement temperatures, respectively. Epitaxial or coherency stress will result from the strain associated with a mismatch in lattice parameters in the case of heteroepitaxial multilayer films. Stress can also arise from interface reactions leading to, e.g., density and/or bond configuration changes resulting from phase formation. And finally, so-called growth or deposition stresses can result from the non-equilibrium growth conditions associated with various deposition techniques. That is, non-equilibrium growth conditions may lead to density changes, the formation of voids, gas incorporation, etc., and these aspects of the microstructure and composition will determine the stress state of the film. In this last case, the resulting stress is highly dependent on the details of the deposition process. Deposition stresses are also dependent on the film thickness, in general, so the  $\sigma$ 's in equation (1) can be thickness-

dependent as well.

The relationship between the deposition stress, the microstructure and composition, and the deposition conditions of thin films deposited by physical vapor deposition (i.e., evaporation or sputtering) has been the subject of active investigation for many years. In the case of films prepared by sputtering, a number of authors have reported on the affect of such parameters as substrate temperature, working gas pressure, working gas composition, source-to-substrate distance, substrate bias, and angular distribution of adatoms. Though a complete fundamental understanding of the physical mechanisms involved is still lacking, a large body of knowledge has been assembled, some of which was summarized recently by Windischmann [16]. By an analysis of results presented in the literature, he suggests that for low substrate temperatures – where the affects of bulk diffusion are negligible, so that the dynamics of the growth process are dominated by adatom surface mobility – the microstructure and deposition stress in a thin film prepared by sputtering or by ion-assisted deposition is determined chiefly by the normalized momentum delivered to the growing film,  $P_n^* = \gamma (ME)^{1/2}$ , where  $M$  is the mass,  $E$  is the energy, and  $\gamma$  is the energetic particle/adatom flux ratio;  $P_n^*$  is a function of several deposition parameters.

At low  $P_n^*$ , (as in the case of sputtering at high gas pressure, for example, in which case the gas is thermalized [17],) the surface mobility of adatoms is small, so films are characterized by a porous columnar microstructure having large surface roughness [18] (i.e., zone 1 microstructure, according to the structure zone model described by Thornton [19],) and a tensile stress state resulting from the interatomic forces exerted across the gaps between columnar grains [20]. At higher  $P_n^*$  values, the surface mobility of adatoms increases, due to collisions with energetic particles striking the film, and by the fact that arriving adatoms have larger kinetic energies to begin with. With greater adatom mobility, voids collapse to dimensions comparable to the range of interatomic forces and the tensile stress thus reaches a maximum. This is followed by a sharp transition from tensile to compressive stress, which is accompanied by a zone T-type microstructure consisting of tightly packed columns. At these high  $P_n^*$  values, as the size and number of

voids decreases further as the result of large adatom mobility, interatomic forces which would otherwise lead to tensile stress are reduced. Compressive stress results as the film becomes over-dense by the so-called atomic peening effect [21]. Compressive stress may also be due to implanted working gas atoms [22], though conclusive evidence for this latter effect has not been reported.

The affect of gas impurities on the stress in sputtered films was also first reported some years ago, by Stuart [23], who investigated a variety of metal films deposited by triode sputtering. For example, he reported that the stress state in tantalum films changed from compressive to tensile by the introduction of oxygen during sputtering. Subsequent studies ([24] – [28], for example) of the affect of gas impurities on film stress for both sputtered and evaporated films focussed mainly on the properties of relatively thick films of otherwise pure materials, and generally involved the deliberate introduction of reactive gas species (e.g.  $\text{H}_2\text{O}$ ,  $\text{H}_2$ ,  $\text{O}_2$ ) into the vacuum system during deposition. Nonetheless, in all of these investigations the film stress was found to (a) depend strongly on the partial pressure of the impurity gases, and (b) be correlated with the amount of impurity atoms incorporated into the film. However, there remains some discrepancy among the various results, and although several possibilities have been proposed (e.g., lattice distortions due to interstitial impurity atoms, the affect of impurity atoms on adatom mobility,) a clear explanation of the mechanism by which impurity atoms affect film stress has not yet emerged.

### **3. EXPERIMENT**

#### **3.1 FILM GROWTH**

ML films were deposited by DC magnetron sputtering, using argon as the working gas. Planar targets, measuring  $50.8 \times 8.9 \times 0.6$  cm, were used, containing either solid Si of 99.999% purity or Mo of 99.9% purity. In this system, which has been described previously [29], the magnetrons (VacTec, Inc.) are mounted along the diagonal of a square, stainless-steel vacuum chamber, and face upward. The substrate is mounted facing downward on a platen that spins as it rotates over each magnetron source (vertical target to substrate distance is 90 mm), thereby building up the multilayer one layer per pass. The spin motion,

which is used to enhance coating uniformity, is driven by a DC motor, and operates at approximately 235 rpm, whereas the rotation motion is driven by a computer-controlled stepper-motor with gear reduction, and operates at any desired rotation rate between 0.00003 and 5.5 rpm. The individual layer thicknesses in the multilayer are thus adjusted by controlling the rotation speed independently over each source, while keeping the intrinsic source deposition rates constant by maintaining constant source power and gas pressure. Stainless steel shielding is used to limit the angular range of deposition, and also serves to minimize cross-contamination between the two sources. The temperature of the substrate was not controlled during deposition.

The deposition chamber was evacuated to a pressure of 0.4 torr with a rotary piston pump. High vacuum was then achieved using a cryopump (CTI model CT-10; pumping speed = 3000 l/s for air, 9000 l/s for water.) The pressure in the chamber was measured using a Bayard-Alpert type ionization gauge (Granville-Phillips model 274 gauge and model 307 controller); the composition of the background gas was also measured during a separate run with a residual gas analyzer (RGA) (Leybold Quadrex 200 with electron multiplier). Accurate partial pressures of background gas components were determined by calibrating the RGA using a controlled leak of  $N_2$ . Figure 1(a) shows the RGA spectra vs. time; Fig. 1(b) shows the partial pressures of the predominant residual gas components vs. time computed from these data, as well as the total pressure computed from the sum of the partial pressures. The apparent total pressure measured with the ion gauge is also shown in Fig. 1(b); the pressure measured with the ion gauge is generally lower than the true pressure (sum of the partial pressures) because the ion gauge controller is calibrated for  $N_2$ , whereas the predominant component of the background gas is water vapor, as indicated in the RGA spectra. The RGA spectra reveal that lesser quantities of hydrogen, nitrogen and/or carbon monoxide, and oxygen are present in the background gas as well.

We maintained precisely the argon pressure during deposition with a closed-loop feedback system consisting of a mass-flow controller (MKS model 2259C) and a capacitance manometer (MKS model

390HA), using Ar of 99.998% purity. The Ar pressure was thus maintained at 1.5 mTorr (0.2 Pa) during deposition (Ar flow rate of ~230 sccm). Power to each magnetron source was supplied by a 1 kW power supply (Advanced Energy model 2011), operated in the regulated power mode at 200 W; typical voltages were ~300 V. The power supplies were ramped to full power over a period of two minutes, with an additional 20-minute warm-up period prior to film growth. The substrate was electrically grounded.

Under the conditions just described, the deposition rates for Mo and Si were measured to be 0.25 and 0.18 nm/s, respectively. ML films containing 40 periods of ~6.9-nm-thick Mo/Si bilayers were deposited onto Si (100) wafer sections measuring  $\sim 16 \times 16 \text{ mm}^2$ , of nominal 100  $\mu\text{m}$  thickness. The native  $\text{SiO}_2$  layer was not removed from the wafers. Three different combinations of individual Mo and Si layer thicknesses were chosen:  $[d_{\text{Si}}, d_{\text{Mo}}] = [4.3 \text{ nm}, 2.6 \text{ nm}]$ , i.e.  $\Gamma = 0.625$ ;  $[3.5 \text{ nm}, 3.5 \text{ nm}]$ , i.e.  $\Gamma = 0.5$ ; and  $[2.6 \text{ nm}, 4.3 \text{ nm}]$ , i.e.  $\Gamma = 0.375$ , where  $\Gamma \equiv d_{\text{Si}} / (d_{\text{Mo}} + d_{\text{Si}})$ . The first layer deposited was Mo and the last Si. The deposition times were of order 40 minutes, depending on the  $\Gamma$  value.

MLs were deposited at various background pressures by varying the pumpdown time, i.e., the elapsed time between the opening of the gate valve isolating the cryopump and the start of the magnetron source warm-up period and subsequent film growth. The pumpdown time was thus varied from ~30 minutes for films deposited at an apparent pressure of  $\sim 1.0 \times 10^{-5}$  torr, up to a period of several days for films deposited at the lowest background pressures. For most samples, the ionization gauge was turned on during the entire pumpdown period (and turned off during deposition.) However, one set of MLs was prepared for which the ion gauge was intentionally left off during pumpdown, except during a three minute period just prior to the magnetron source warm-up (so that the background pressure could be measured.) We note that for films deposited at the highest pressures, the deposition time is comparable to the pumpdown time; considering the data of Fig. 1(b), it is clear that the partial pressures of the background gases must have dropped significantly during the course of the deposition for these samples. Unfortunately, due to the configuration of the system, it was not possible to obtain RGA data during deposition.

### 3.2 FILM CHARACTERIZATION

If a film of thickness  $t_f$  having a biaxial stress  $\sigma$  is attached to a substrate of thickness  $t_s$ , it will cause the substrate to deform, as required by the condition of static equilibrium. If the substrate is very much thicker than the film, the deformation will be spherical, having a radius of curvature  $R$ . The relationship between  $\sigma$  and  $R$  is given by the well-known Stoney equation [30]:

$$(3) \quad \sigma = \frac{Y_s t_s^2}{6 t_f} \frac{1}{R}$$

where  $Y_s$  is the biaxial elastic modulus of the substrate (which is related by  $Y_s = E_s / (1 - \nu_s)$  to  $E_s$ , Young's modulus, and  $\nu_s$ , Poisson's ratio for the substrate.) A measurement of the radius of curvature  $R$  can thus be used to infer the stress in the film, assuming that the the elastic properties of the substrate and the thicknesses are known. By convention, positive  $\sigma$  refers to a tensile stress state, in which the substrate is bowed towards the film (concave), while negative  $\sigma$  corresponds to a compressive stress state, in which the substrate is bowed away from the film (convex).

ML stress was thus measured using the wafer curvature technique, with a laser-scanning apparatus that has been described previously [31]. With this apparatus, wafer curvature is determined by measuring the deflection of a HeNe laser beam as it scans along the surface of the sample. The curvature resulting from the stress in the film is computed by measuring the wafer curvature before and after deposition. From the measured curvature, the film stress is computed using equation (3). Substrate thicknesses were measured with a micrometer, and film thicknesses determined from X-ray diffraction (described below.) A value of 180 GPa for  $Y_s$  was used [32]. We estimate that the stress measurements are accurate to  $\pm 5\%$ .

In addition to the wafer curvature measurements, the microstructure of selected samples was characterized using a variety of X-ray techniques, and film composition was investigated by both Auger electron spectroscopy (AES) and forward-recoil-scattering (FRS). With the exception of the FRS measurements, characterization was limited to selected  $\Gamma = 0.625$  ML films.

X-ray diffraction measurements were made at a wavelength of 0.154 nm (Cu K- $\alpha$ ) using a four-

circle diffractometer fitted with a rotating anode source and a pyrolytic graphite crystal monochromator. Small angle measurements (from 0 to 8° grazing) in the  $\theta$ - $2\theta$  geometry were used to measure the Bragg peaks resulting from the ML periodicity (i.e.,  $d \sim 6.9$  nm), while large angle measurements (from  $2\theta = 30$  to 50°), also in the  $\theta$ - $2\theta$  geometry, were used to examine the Mo (110) diffraction peaks. From the small angle measurements, the individual layer thicknesses (and therefore the deposition rates) were determined with high precision, by fitting the measured data with calculations based on recursive application of the Fresnel equations [33]. Non-specular X-ray scattering measurements were also made, in this case by varying the detector angle ( $2\theta$ ) while maintaining a fixed incidence angle (corresponding to the first Bragg peak, i.e.,  $\theta = 0.73^\circ$ ), in order to measure any intensity variations in the Yoneda peaks that would result from different amounts of correlated interfacial roughness [34].

The absolute soft X-ray reflectance was measured using a laser-plasma-based reflectometer system that has been described previously [33]. The reflectance was measured versus wavelength from 12 to 15.5 nm, in 0.5 nm increments, at a fixed incidence angle of 3° from normal.

Oxygen and carbon concentrations were determined from AES measurements made with a PHI 595 system (Perkin-Elmer). Depth profiling was achieved by sputtering with a 4 KeV argon beam. Hydrogen concentrations were determined from FRS measurements using a 2.6 MeV He beam, at 15° grazing incidence on the samples with the H recoil at 30° to the incident beam direction [35]. He atoms were removed from the forward scattered beam using an 11.8- $\mu\text{m}$ -thick Mylar foil, and recoil H atoms were measured with a silicon surface barrier detector. The average concentration of hydrogen in selected ML samples was determined by taking the ratio of the number of forward recoil H events measured for each sample, at a fixed dose of 40  $\mu\text{C}$  of beam, to the number of counts obtained from a calibration sample of Si containing  $5 \times 10^{15}$  atoms/ $\text{cm}^2$  of implanted hydrogen. As a result of the uncertainty associated with the application of the pure Si calibration sample to a ML film, we estimate that the hydrogen concentrations reported in the next section are only accurate to  $\pm 10\%$ . However the precision of these measurements (i.e., resulting from

the uncertainty associated with the H counting statistics) is much better, in the range of  $\pm 1 - 2\%$ , depending on the sample.

#### 4. RESULTS

Shown in Figure 2 are the stresses measured in Mo/Si ML films as a function of background pressure. As can be seen from this plot, the compressive stress in these films varies ~linearly with the log of the background pressure: for the  $\Gamma = 0.625$  films, the compressive stress decreases from approximately  $-450$  MPa to  $-250$  MPa as the apparent background pressure in the deposition chamber (measured with the ion gauge just prior to deposition) increases from  $6.0 \times 10^{-8}$  to  $1.0 \times 10^{-5}$  torr. For the  $\Gamma = 0.5$  and  $\Gamma = 0.375$  samples, the stress variation is even more strongly dependent on background pressure. (We note that for a given background pressure, the stress becomes more tensile with decreasing  $\Gamma$ , i.e. with increasing Mo layer thickness: evidently the Mo layers are in tension, and the Si layers in compression.) Also shown in Fig. 2 are the stress-vs-background-pressure data for the ( $\Gamma=0.625$ ) samples deposited with the ion gauge off during pumpdown. The stresses for these samples are approximately 30 MPa more compressive than for the equivalent samples deposited with the ion gauge turned on during pumpdown.

Figure 3 shows representative X-ray and soft X-ray data, comparing the results obtained for high-background-pressure/low-compressive-stress versus low-background-pressure/high-compressive-stress  $\Gamma=0.625$  MLs. The only significant difference in these data between the low-stress and high-stress films is in the appearance of the three ML diffraction peaks [Fig. 3(a)] measured at the largest angles, i.e., between  $5.5$  and  $7.5^\circ$ : these peaks are sharper, and more intense for the high-compressive-stress sample. By fitting these curves, we attribute this to a difference of  $\sim 0.2$  nm in interfacial roughness between these two films. In contrast, the peak soft X-ray reflectances [Fig. 3(b)] of the two samples are identical within experimental uncertainty, aside from a slight wavelength shift resulting from a small difference in ML period. (This difference in ML period is due to a drift in the deposition rate from run-to-run, and was determined to be uncorrelated with background pressure.) The non-specular scattering curves [Fig. 3(c)] indicate that there

are no significant differences in the amount of light scattered into the Yoneda peaks [36], suggesting no differences in the correlated interfacial roughness in these structures. The widths of the Mo (110) peaks in the large-angle X-ray diffraction data [Fig. 3(d)] are also identical for the two samples, indicating no differences in the average grain size along the growth direction of the Mo crystallites in these films, which we infer from these widths to be  $\sim 2.9 \pm 0.2$  nm [37] (i.e., comparable to the thickness of the Mo layers in these samples.) From the location of these peaks (i.e.,  $2\theta = 40.54^\circ$ ) we can discern no differences in the average out-of-plane {110} interplanar spacing between the two films. However, the sensitivity of these measurements to variations in the in-plane stress is not great: assuming that the relative locations of the (110) peaks can be determined with a precision of  $0.05^\circ$ , corresponding to an uncertainty in the average (out-of-plane) interplanar spacing of 0.0005 nm, the smallest strain that can be measured is thus  $\sim 2.3 \times 10^{-3}$ . Using the elastic constants for bulk Mo from reference [38], this corresponds to an in-plane biaxial stress of  $\sim 900$  MPa, larger than any of the stresses we have measured.

The small-angle X-ray scattering measurements, the non-specular X-ray scattering measurements, and the soft X-ray reflectance measurements are each sensitive to particular aspects of the interface morphology of the MLs studied here. The soft X-ray reflectance measurements are sensitive to both interfacial diffuseness and to interfacial roughness over spatial wavelengths from about 1  $\mu\text{m}$  to 10 nm [39]. The small-angle X-ray data is also sensitive to diffuseness, and to roughness over a larger range of spatial wavelengths, from about 5  $\mu\text{m}$  to 0.15 nm, though the affect of interfacial roughness on the X-ray reflectance [Fig. 3(a)] is greatest at the largest grazing angles. The heights of Yoneda peaks evident in the non-specular scattering data, on the other hand, are sensitive only to *correlated* interfacial roughness at short spatial wavelengths (from 0.15 nm to 0.15  $\mu\text{m}$ , depending on  $2\theta$ .) Therefore, because the only significant difference between the high-compressive-stress and low-compressive-stress MLs evident in the X-ray data is the sharper and more intense ML Bragg peaks observed in the low-angle X-ray data, we conclude that the high-compressive-stress MLs have slightly reduced uncorrelated, high-frequency (i.e.,

spatial wavelengths between 0.15-10 nm) interfacial roughness.

AES measurements detected only trace quantities ( $\sim 0.5$  at.%) of oxygen in both high-stress and low-stress MLs, with no measurable differences between the two. Furthermore, no carbon was detected (instrumental limit of  $\sim 0.1$  at.%) in either film. However, as can be seen from the FRS data in Figure 4, the hydrogen concentration was found to depend strongly on both the background pressure and the relative thickness of the Mo layers.

Shown in Fig. 4(a) are FRS spectra for three representative samples: two  $\Gamma=0.625$  MLs, one deposited at  $1.1 \times 10^{-7}$  torr, and the other at  $1.0 \times 10^{-5}$  torr, and a  $\Gamma=0.5$  ML deposited at  $1.5 \times 10^{-5}$  torr. For these spectra lower H energy corresponds to greater depth into the films. The peak at channel  $\sim 395$  arises from H at the film surface, present as adsorbed gas or as hydrocarbons due to exposure to room air. The film-substrate interface is centered at approximately channel 250. As can be seen from these curves, the average H concentration increases with increasing background pressure (as indicated by the relative areas under the curves.) We also note that the distribution of H is not uniform in the films, but increases with depth into the film, as indicated by the rise in counts from just below the surface H peak towards the film-substrate interface. Presumably the decrease in H concentration as the film is deposited is a result of the normal reduction in background pressure with time [Fig. 1(b)], enhanced by the gettering action of the Mo and Si deposited on the internal surfaces of the deposition system.

Shown in Fig. 4(b) are the average H concentrations (through the film thickness)  $\langle n_H \rangle$  deduced from the FRS spectra for three  $\Gamma=0.625$  MLs. Since the FRS results indicate that the change in H concentration is linear with background pressure [at least for the  $\Gamma=0.625$  MLs shown in Fig. 4(b)], it follows that the change in ML stress also scales linearly with the log of the H concentration. Shown in Fig. 4(c) is the total hydrogen (i.e., H atoms/cm<sup>2</sup>) as a function of  $\Gamma$ , for three films deposited in the range  $1.0 - 1.8 \times 10^{-5}$  torr. Evidently the hydrogen is incorporated preferentially in the Mo layers: if we assume that the total hydrogen scales linearly with  $\Gamma$ , as indicated by the best fit straight line in Fig. 4(c), then we deduce that

the H concentrations in the individual layers are  $\langle n_{\text{H}} \rangle_{\text{Mo}} = 2.2 \pm 0.1$  at.% for the Mo, and  $\langle n_{\text{H}} \rangle_{\text{Si}} = 0.4 \pm 0.3$  at.% for the Si layers deposited in this background pressure range.

Using the stress-vs-background-pressure-vs- $\Gamma$  results presented in Fig. 2, we can estimate the contribution from the individual layers to the total variation in stress with pressure. The variation in ML stress with background pressure is given by

$$(4) \quad \sigma'_{\text{ML}}(\Gamma) = \Gamma \sigma'_{\text{Si}} + (1 - \Gamma) \sigma'_{\text{Mo}},$$

obtained by differentiating equation (1) (and neglecting the interfacial stress term.) In this expression we are using the abbreviated notation for the derivative of stress with respect to the log of the background pressure  $P$ , i.e.,  $\sigma' \equiv d\sigma(P) / d \log P$ . Although the values for  $\sigma_{\text{Si}}$  and  $\sigma_{\text{Mo}}$  depend, in general, on  $d_{\text{Si}}$  and  $d_{\text{Mo}}$ , respectively, it is reasonable to assume that the derivatives with respect to background pressure of these quantities, i.e.,  $\sigma'_{\text{Si}}$  and  $\sigma'_{\text{Mo}}$ , are independent of thickness over the range of layers thicknesses investigated here. Thus, using for  $\sigma'_{\text{ML}}$  the slopes of the three stress-vs-background-pressure curves presented in Fig. 2, there are three ways we can solve this system of three equations for the two unknown quantities  $\sigma'_{\text{Si}}$  and  $\sigma'_{\text{Mo}}$ . We find that  $\sigma'_{\text{Si}} = -220 \pm 11$  MPa/log(Torr) and  $\sigma'_{\text{Mo}} = 560 \pm 11$  MPa/log(Torr), where the uncertainties in these values refer to the standard deviations about the mean values for the three sets of slope values. So, according to this analysis, the change in stress in the  $\Gamma = 0.5$  ML films, for example, associated with the increase in background pressure from  $3.3 \times 10^{-7}$  to  $1.5 \times 10^{-5}$  torr would be the result of the Si layers becoming more compressive by  $\sim 340$  MPa, and the Mo layers more tensile by  $\sim 850$  MPa. Thus, the stresses in the tensile Mo layers and the compressive Si layers both increase with increasing background pressure, and the contribution of the Mo layers to the change in ML stress with background pressure is  $\sim 2.5$  times greater than that of the Si layers.

## 5. DISCUSSION

The variation in ML stress with background pressure is most likely due in some way to the reactive gas species present in the background gas and observed with the RGA (Fig. 1), i.e., hydrogen, oxygen, water, etc., as an increase in the partial pressures of these gases is correlated with an increase in tensile stress in the MLs. Because of this correlation, we attribute our observation that the ML stress is more tensile when the ion gauge

is turned on during pumpdown to an increase in the partial pressures of the residual gases that affect the film stress most strongly, as a result of enhanced electron and ion stimulated desorption from the walls of the vacuum chamber [40].

Therefore, and in light of the discussion of the origins of deposition stresses in sputtered films presented in section 2, the most likely explanations for the observed variation in ML stress with background pressure are: (1) adsorption of impurity atoms on the surface of the film affects a number of parameters that can influence the growth process, including the surface mobility of adatoms, the probability of adatom adsorption, and the density of available surface sites; and (2) the increase in tensile stress is due to an increase in impurity atom incorporation in the film. We discuss each of these possibilities in turn.

The surface mobility of adatoms can also be affected by adsorbed gas atoms, by a variety of possible mechanisms [19], [28], [41]. Regardless of the details of the specific mechanisms that may be involved, we note that as the background gas partial pressure increases, the ratio of the number of residual gas atoms striking the film to the number of sputtered atoms being added to the film also increases; at the highest background gas pressures considered here, i.e.,  $1 \times 10^{-5}$  Torr, this ratio is of order 5 [42]. It seems likely, therefore, that the observed variation in stress with background pressure is due, at least partially, to a chemically induced reduction in adatom surface mobility resulting from adsorbed residual gas atoms. We also note that our observation of increased interfacial roughness in films deposited at the highest background pressures is consistent with the tendency towards a zone 1 microstructure (and corresponding tensile stress state) associated with reduced adatom mobility [41]. In particular, the increased roughness may be indicative of changes in the distribution or size of the Mo grains in the plane of the film (i.e., that were not detected by the X-ray diffraction measurements described above,) which could be the cause of the change in stress [20]. It may also be possible that adsorbed residual gas atoms affect in some way the formation of the mixed Mo-Si interlayers in these films, thereby affected any interfacial stresses that may be present. However, we have no evidence that there are any such stresses, so we cannot estimate quantitatively how the residual gas atoms might have an effect.

As described in section 2, incorporation of impurity atoms in sputtered films is known to affect film stress, though the exact mechanism by which this occurs has not been determined conclusively. In our case, we

find very little incorporated oxygen and carbon; distortion of the Mo lattice, as was reported for the Mo films containing oxygen impurities investigated by Yamaguchi and Miyagawa [27], was not observed in any of our films as well. We do, however, find a strong correlation between film stress and incorporated hydrogen: the ML stress varies as the log of the average hydrogen concentration; this functional dependence has not, to our knowledge, been reported previously. Our conclusion that the Si layers become more compressive with increasing background pressure is consistent with similar observation in a-Si:H films reported by Windischmann *et al* [26]. It seems likely, therefore, that the incorporated hydrogen is at least partly responsible for the observed variation of stress with background pressure.

## 6. CONCLUSIONS

We have measured the stress in Mo/Si ML films deposited by magnetron sputtering and find that the stress in these films becomes increasingly tensile with increasing background pressure. The variation in the dependence of film stress with background pressure as a function of relative Mo-layer thickness suggests that while the Mo layers become more tensile with increasing background pressure, the Si layers become more compressive. We find that the variation in ML stress correlates with the concentration of incorporated hydrogen in these films, i.e., increasing hydrogen concentrations correspond to more tensile films. The concentration of hydrogen varies linearly with background pressure, and is also correlated with the relative thickness of the Mo layers in these structures, indicating that hydrogen is located preferentially in the Mo layers. The concentrations of oxygen and carbon were found to be very small, and were uncorrelated with stress. The only evidence for microstructural variations in these films was a slight increase in the uncorrelated, high-frequency interfacial roughness with increasing background pressure (as determined from small-angle X-ray scattering,) suggesting a tendency towards tensile, zone 1-type microstructure with increasing background pressure.

The most likely explanations for the observed variation in ML stress with background pressure are first, that the stress is due to incorporation of hydrogen atoms, and second, that the surface mobility of adatoms is decreased with increasing background pressure, most likely due to the affect of adsorbed residual gas atoms. From our measurements alone we cannot provide any further information regarding the details of how these two possible mechanisms affect film stress.

We note that Mo/Si MLs ( $\Gamma=0.625$ ,  $d=6.9$  nm) deposited at high background pressure still show high soft X-ray reflectance. This implies that the stress in such films can and should be minimized by controlling the background pressure, or perhaps by the deliberate introduction of impurity gases, in order to reduce the deformation of the substrate in X-ray imaging applications such as projection lithography. Our results also indicate that the background pressure of the deposition system must be controlled in order to produce low-stress films with good repeatability. Indeed, the dependence of stress on background pressure may be the cause of the scatter in some of the stress data reported in the literature [43], [44].

### **ACKNOWLEDGMENTS**

The authors kindly thank R. Opila for the AES measurements.

## REFERENCES

- [1] B. M. Clemens and R. Sinclair, *Mat. Res. Soc. Bulletin*, **XV**, 19-28 (1990), and references therein
- [2] I. K. Schuller, J. Guimpel, and Y. Bruynseraede, *Mat. Res. Soc. Bulletin*, **XV**, 29-36 (1990), and references therein
- [3] J. E. Bjorkholm, J. Bokor, L. Eichner, R. R. Freeman, J. Gregus, T. E. Jewell, W. M. Mansfield, A. A. MacDowell, E. L. Raab, W. T. Silfvast, L. H. Szeto, D. M. Tennant, W. K. Waskiewicz, D. L. White, D. L. Windt, and O. R. Wood, II, *J. Vac. Sci. Tech. B.*, **8**, 1509-1513 (1990)
- [4] J. B. Kortright and J. H. Underwood, *Nuc. Inst. Meth. Phys. Res. A*, **291**, 272-277 (1990)
- [5] J. B. Kortright and R. S. DiGennaro, *Rev. Sci. Instrum.*, **60**, 1995-1998 (1989)
- [6] C. M. Falco and I. K. Schuller, in *Synthetic Modulated Structures*, edited by L. L. Chang and B. C. Giessen (Academic Press, Orlando, FL, 1985), p. 339-364
- [7] T. W. Barbee, *Mat. Res. Soc. Bulletin*, **XV**, 37-44 (1990), and references therein
- [8] J. A. Thornton and D. W. Hoffman, *J. Vac. Sci. Tech.* **14**, 164-168 (1977)
- [9] D. L. Windt, R. R. Kola, W. K. Waskiewicz, R. Hull, J. Griffith, and D. A. Grigg, *Tech. Dig. Opt. Soc. Amer.* **7**, 12-15 (1992)
- [10] R. R. Kola, D. L. Windt, W. K. Waskiewicz, B. E. Weir, R. Hull, G. K. Celler and C. A. Volkert, *App. Phys. Lett.*, **60**, 3120-3122 (1992)
- [11] A. K. Petford-Long, M. B. Stearns, C. H. Chang, S. R. Nutt, D. G. Stearns, N. M. Ceglio, and A. M. Hawryluk, *J. Appl. Phys.*, **61**, 1422 (1987); K. Holloway, K. B. Do, and R. Sinclair, *J. Appl. Phys.*, **65**, 474 (1989); D. G. Stearns, M. B. Stearns, Y. Cheng, J. H. Stith, and N. Ceglio, *J. Appl. Phys.*, **67**, 2415 (1990); R. S. Rosen, M. A. Viliardos, D. G. Stearns, M. E. Kassner, and S. P. Vernon, *Proc. SPIE*, **1547**, 212 (1991); D. L. Windt, R. Hull, and W. K. Waskiewicz, *J. Appl. Phys.*, **71**, 2675-2678 (1992)
- [12] J. W. Cahn and F. Larche, *Acta Metall.*, **30**, 51-56 (1982)
- [13] J. A. Ruud, A. Witvrouw, and F. Spaepen, *J. Appl. Phys.*, **74**, 2517-2523 (1993)

- [14] J. A. Bain, L. J. Chyung, S. Brennan, and B. M. Clemens, *Phys. Rev. B*, **44**, 1184-1192 (1991)
- [15] W. D. Nix, *Metal. Trans. A*, **20A**, 2217-2245 (1989)
- [16] H. Windischmann, *J. Vac. Sci. Tech. A*, **9**, 2431-2436 (1991)
- [17] R. E. Somekh, *J. Vac. Sci. Technol. A*, **2**, 1285-1291 (1984)
- [18] G. S. Bales and A. Zangwill, *J. Vac. Sci. Technol. A*, **9**, 145-149 (1991)
- [19] J. A. Thornton, *J. Vac. Sci. Technol.*, **11**, 666-670 (1974)
- [20] F. A. Doljack and R. W. Hoffman, *Thin Solid Films*, **12**, 71-74 (1972)
- [21] F. M. D'Heurle, *Metall. Transactions*, **1**, 725-732 (1970)
- [22] C. C. Fang, F. Jones, and V. Prasad, *J. Appl. Phys.*, **74**, 4472-4482 (1993)
- [23] P. R. Stuart, *Vacuum*, **19**, 507-511 (1969)
- [24] P. M. Alexander and R. W. Hoffman, *J. Vac. Sci. Technol.*, **13**, 96-98 (1976)
- [25] R. A. Roy and R. Messier, *J. Vac. Sci. Technol. A*, **2**, 312-315 (1984)
- [26] H. Windischmann, R. W. Collins, and J. M. Cavese, *J. Non-crystalline Solids*, **85**, 261-272 (1986)
- [27] T. Yamaguchi and R. Miyagawa, *Jap. J. Appl. Phys.*, **30**, 2069-2073 (1991)
- [28] R. Abermann, *Mat. Res. Soc. Symp. Proc.*, **239**, 25-37 (1992)
- [29] D. L. Windt and W. K. Waskiewicz, *J. Vac. Sci. Technol. B*, **12**, ??-?? (1994)
- [30] G. G. Stoney, *Proc. Roy. Soc. London*, **A82**, 172-175 (1909)
- [31] C. A. Volkert, *J. Appl. Phys.*, **70**, 3251-3257 (1991)
- [32] W. A. Brantley, *J. Appl. Phys.*, **44**, 534 (1973)
- [33] D. L. Windt and W. K. Waskiewicz, *Proc. SPIE*, **1547**, 144-158 (1991)
- [34] D. G. Stearns, *J. Appl. Phys.*, **71**, 4286-4298 (1992)
- [35] L. C. Feldman and J. W. Mayer, *Fundamentals of Surface and Thin Film Analysis*, (Elsevier Science Pub. Co. Inc., New York, 1986)

- [36] Yoneda, *Phys. Rev.*, **131**, 2010 (1963)
- [37] B. D. Cullity, *Elements of X-Ray Diffraction*, (Addison-Wesley, Reading, MA, 1987), p. 284
- [38] *Handbook of Tables For Applied Engineering Science*, R. E. Bolz and G. L. Tuve, editors, 1991, CRC Press, Boca Raton, FL
- [39] D. L. Windt, W. K. Waskiewicz and J. E. Griffith, *App. Opt.*, **33**, 2025-2031 (1994)
- [40] M. Andritschky, *Vacuum*, **42**, 753-756 (1991)
- [41] R. Messier, A. P. Giri, and R. A. Roy, *J. Vac. Sci. Technol. A*, **2**, 500-503 (1984)
- [42] C. M. Falco, *J. Appl. Phys.*, **56**, 1218-1219 (1984)
- [43] T. D. Nguyen, X. Lu, and J. H. Underwood, in *The Physics of X-Ray Multilayer Structures*, 1994 Technical Digest Series, Vol. 6 (Optical Society of America, Washington, DC, 1994) pp. 102-105
- [44] R. R. Kola, G. K. Celler, J. Frackowiak, C. W. Jurgensen, and L. E. Trimble, *J. Vac. Sci. Technol. B*, **9**, 3301-3305 (1991)

## FIGURE CAPTIONS

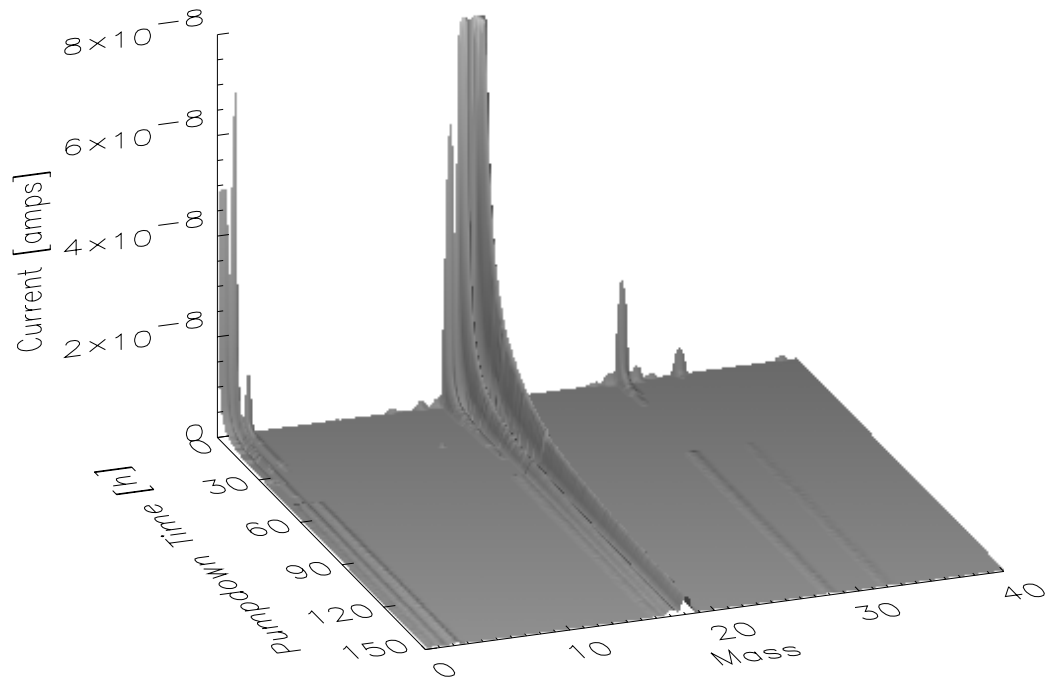
**Figure 1.** (a) Residual Gas Analyzer (RGA) spectra versus pumpdown time. The predominant features correspond to water ( $\text{OH}^+$  and  $\text{H}_2\text{O}^+$ ; masses 17 and 18, respectively), hydrogen ( $\text{H}^+$  and  $\text{H}_2^+$ ; masses 1 and 2, respectively), nitrogen/carbon monoxide ( $\text{N}_2^+$  /  $\text{CO}^+$ ; mass 28), and oxygen ( $\text{O}^+$  and  $\text{O}_2^+$ ; masses 16 and 32, respectively.) (b) Partial pressures of major background gas species versus pumpdown time, computed from the data in (a). The total pressure (dotted), equal to the sum of the partial pressures, and the apparent total pressure measured with an ionization gauge (dashed) are indicated.

**Figure 2.** Measured stress versus background pressure in  $\sim 6.9$ -nm-period multilayer films, with  $\Gamma=0.375$  (squares),  $\Gamma=0.5$  (diamonds), and  $\Gamma=0.625$  (open triangles). Also shown are the data for  $\Gamma=0.625$  ML films for which the ion gauge remained off during pumpdown (filled triangles). The dashed lines are least-squares fits to these data sets.

**Figure 3.** X-ray characterization results for  $\Gamma=0.625$  MLs, comparing high-background-pressure/low-stress (solid) versus low-background-pressure/high-stress (dashed) multilayer films. (a) Small angle, specular X-ray ( $\lambda = 0.154$  nm) reflectance measured in the  $\theta$ - $2\theta$  geometry. The Bragg peaks correspond to the multilayer period  $d \sim 6.9$  nm. (b) Soft X-ray reflectance measured near normal incidence ( $3^\circ$ ) versus wavelength. (c) Non-specular X-ray ( $\lambda = 0.154$  nm) reflectance measured by varying  $2\theta$  at a constant incidence angle  $\theta = 0.73^\circ$ . (d) Large-angle X-ray ( $\lambda = 0.154$  nm) scattering, also in the  $\theta$ - $2\theta$  geometry, comparing the Mo (110) diffraction peaks.

**Figure 4.** (a) FRS spectra for selected ML samples:  $\Gamma = 0.625$ ,  $P = 1.1 \times 10^{-7}$  Torr (solid),  $\Gamma = 0.625$ ,  $P = 1.0 \times 10^{-5}$  Torr (dotted),  $\Gamma = 0.5$ ,  $P = 1.5 \times 10^{-5}$  Torr (dashed). (b) Average hydrogen concentration as a function of background pressure for  $\Gamma=0.625$  MLs, and (c) total hydrogen as a function of  $\Gamma$  for MLs deposited at background pressures in the range  $1.0 - 1.8 \times 10^{-5}$  Torr. The dashed lines in (b) and (c) are least-squares fits to the data.

**a**



**b**

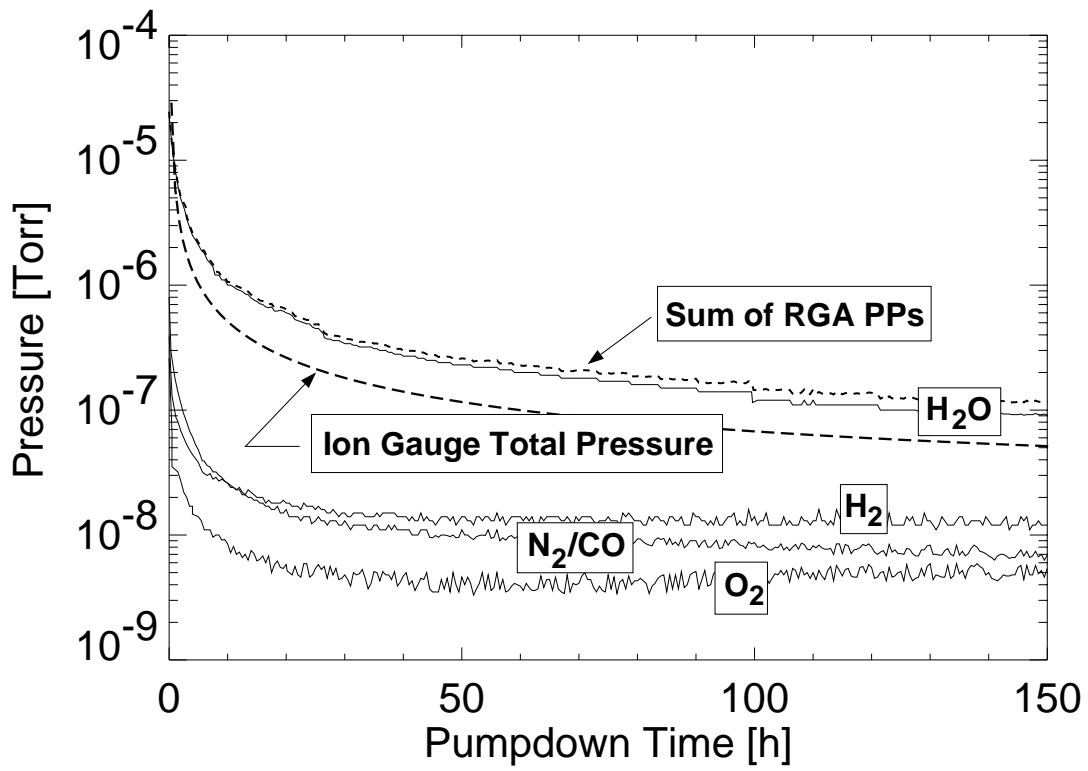


**Figure 1.**

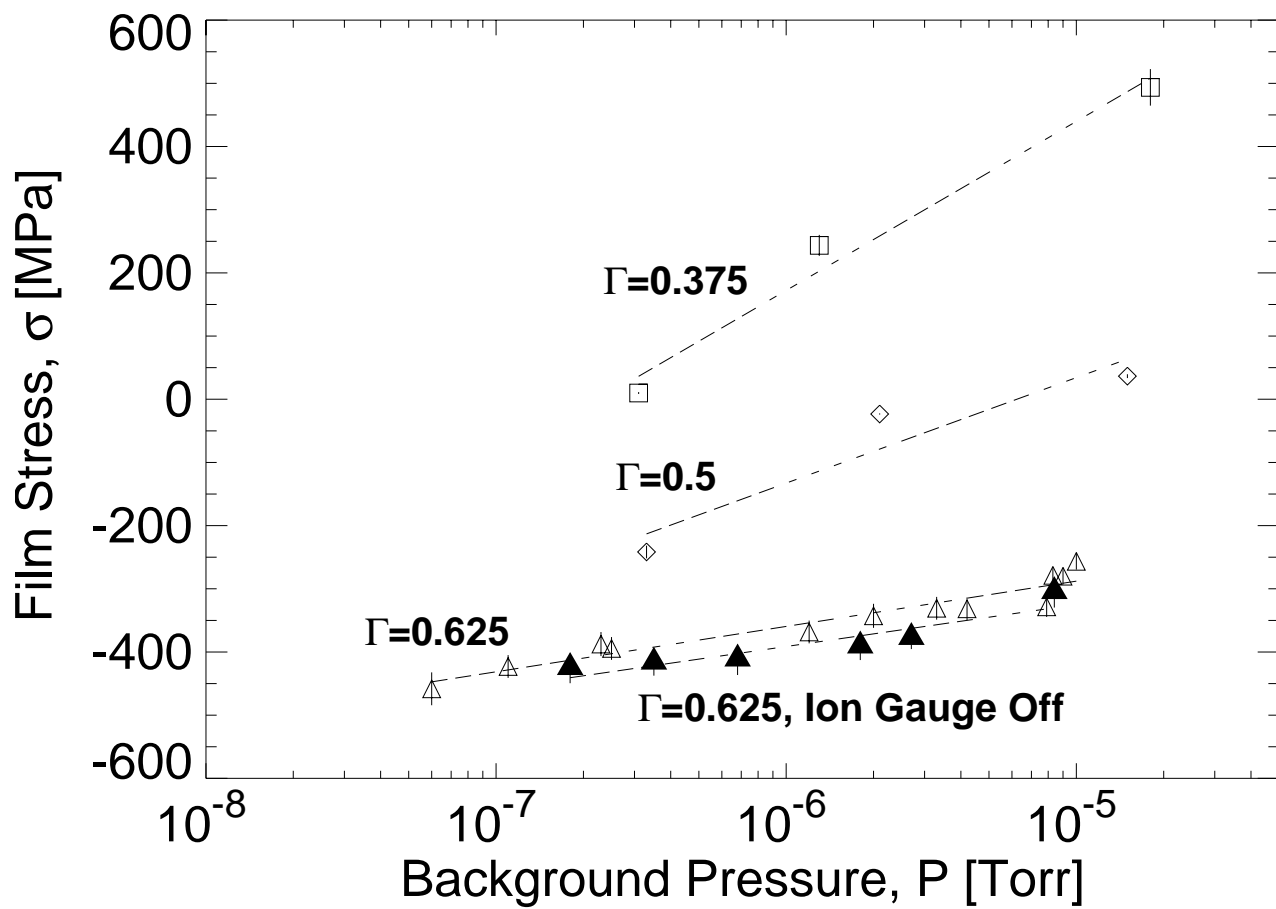
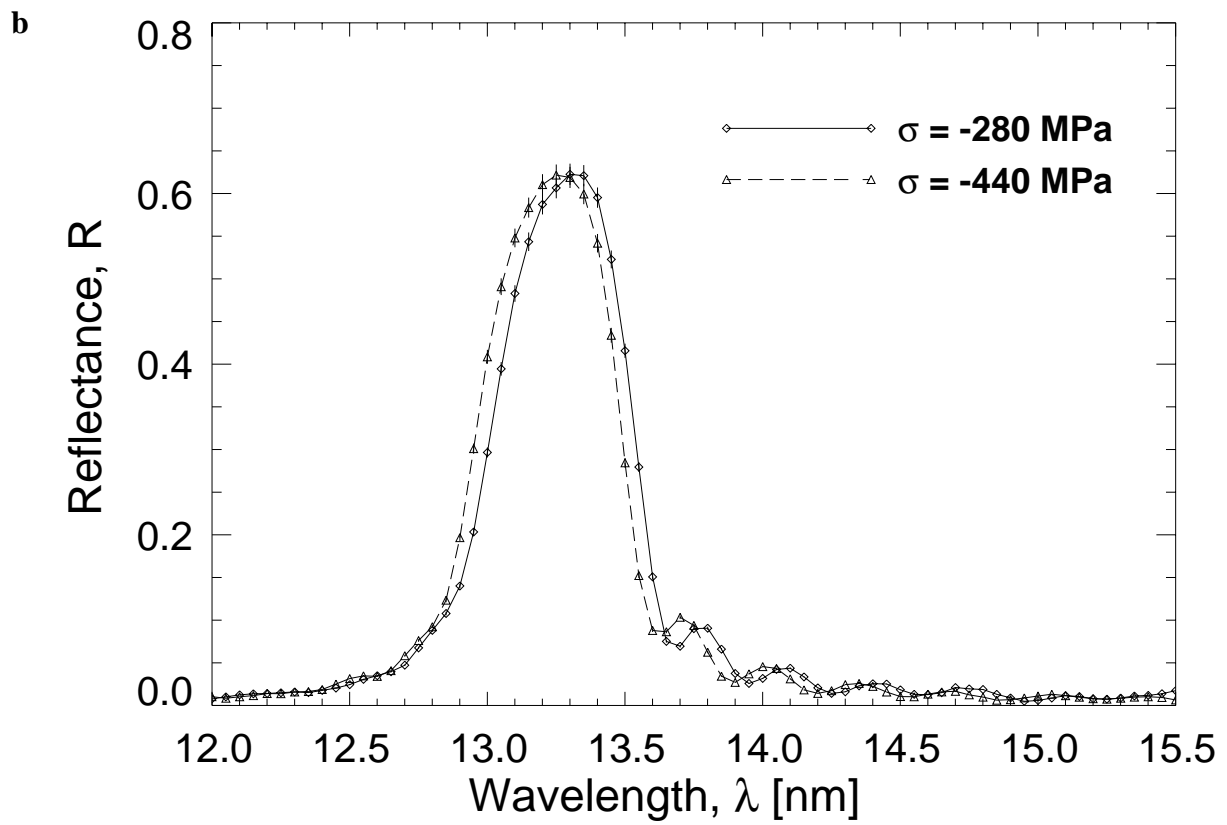
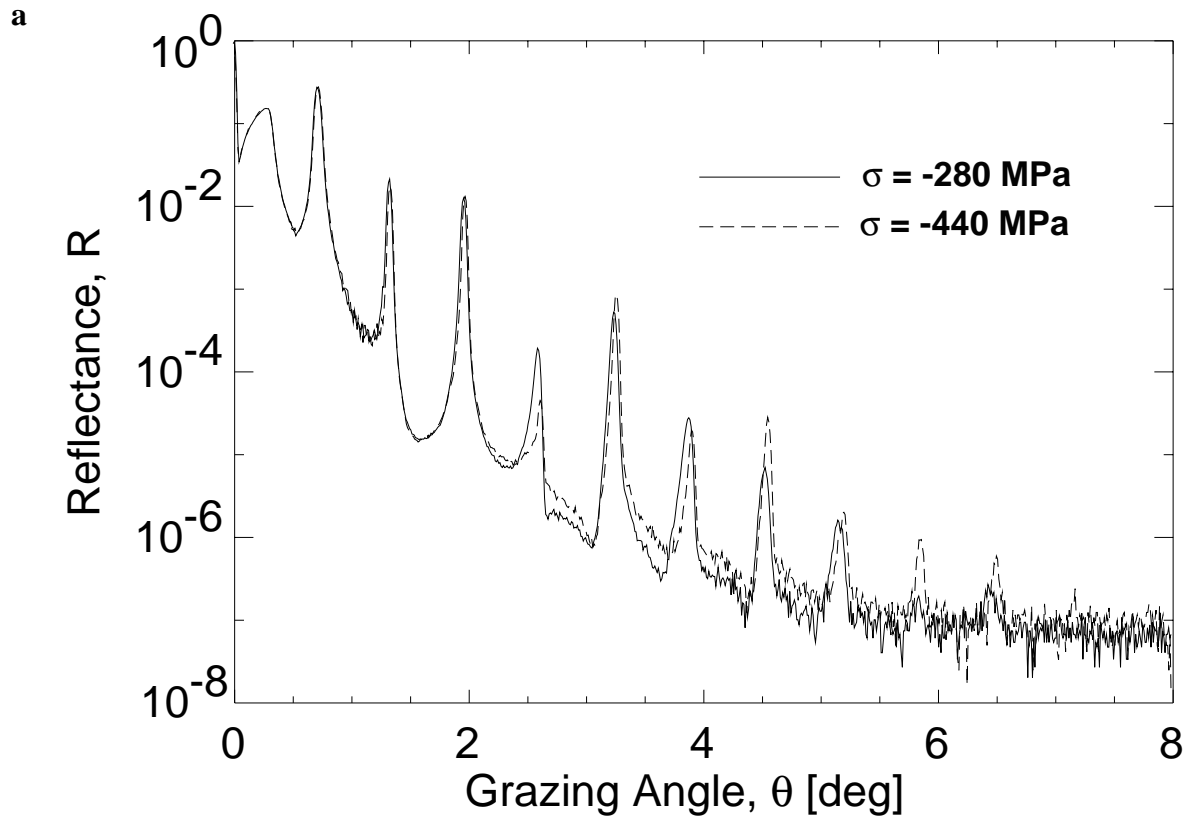
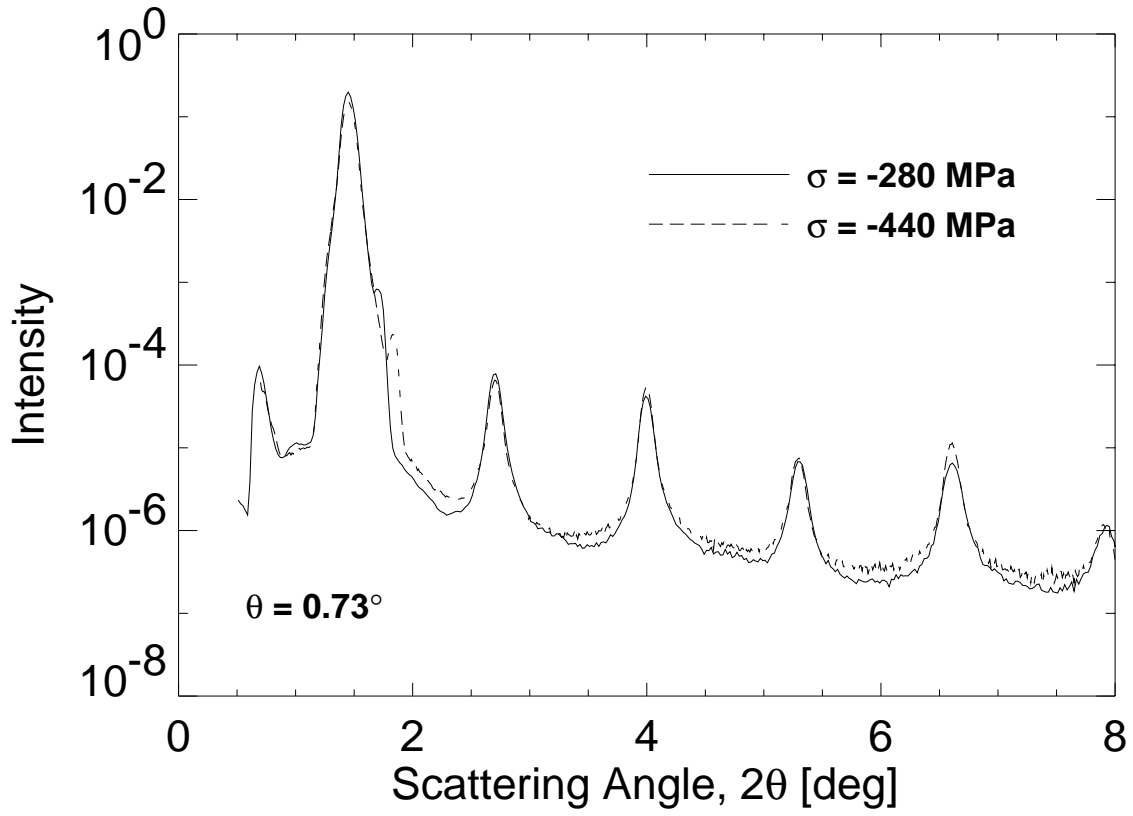


Figure 2.



**Figure 3.**

c



d

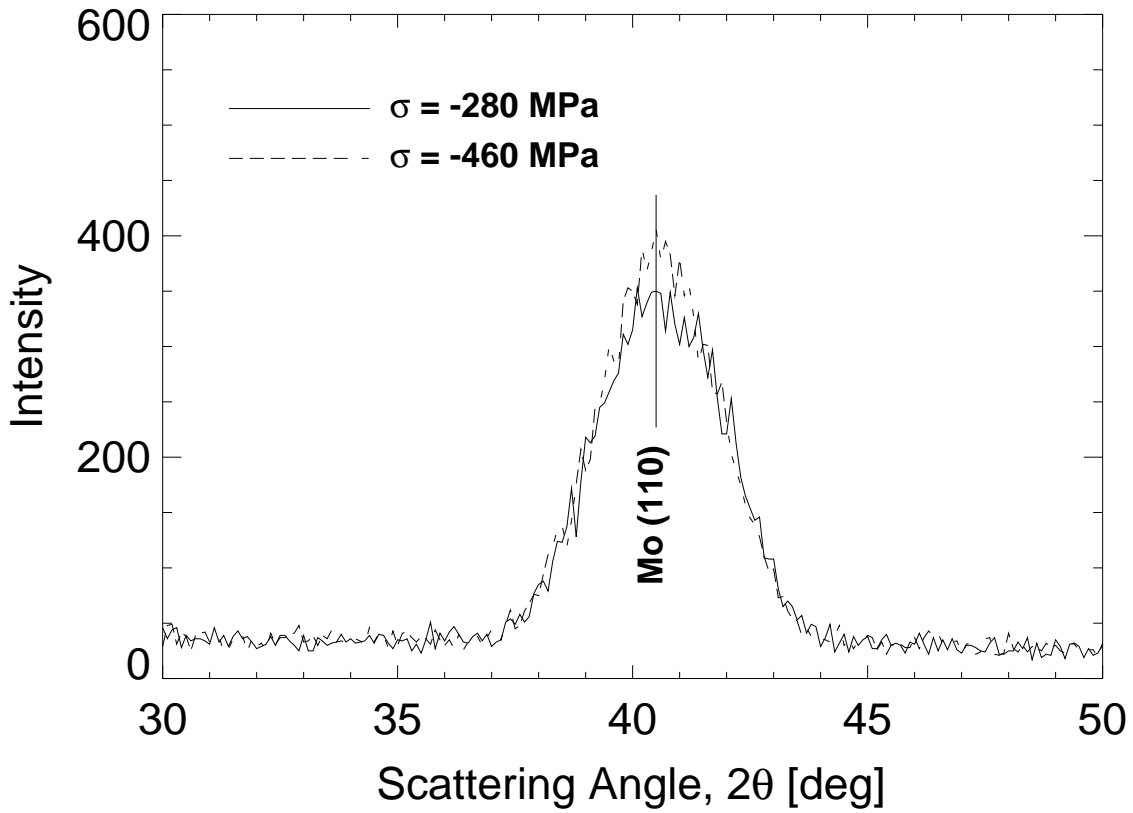


Figure 3. (cont.)

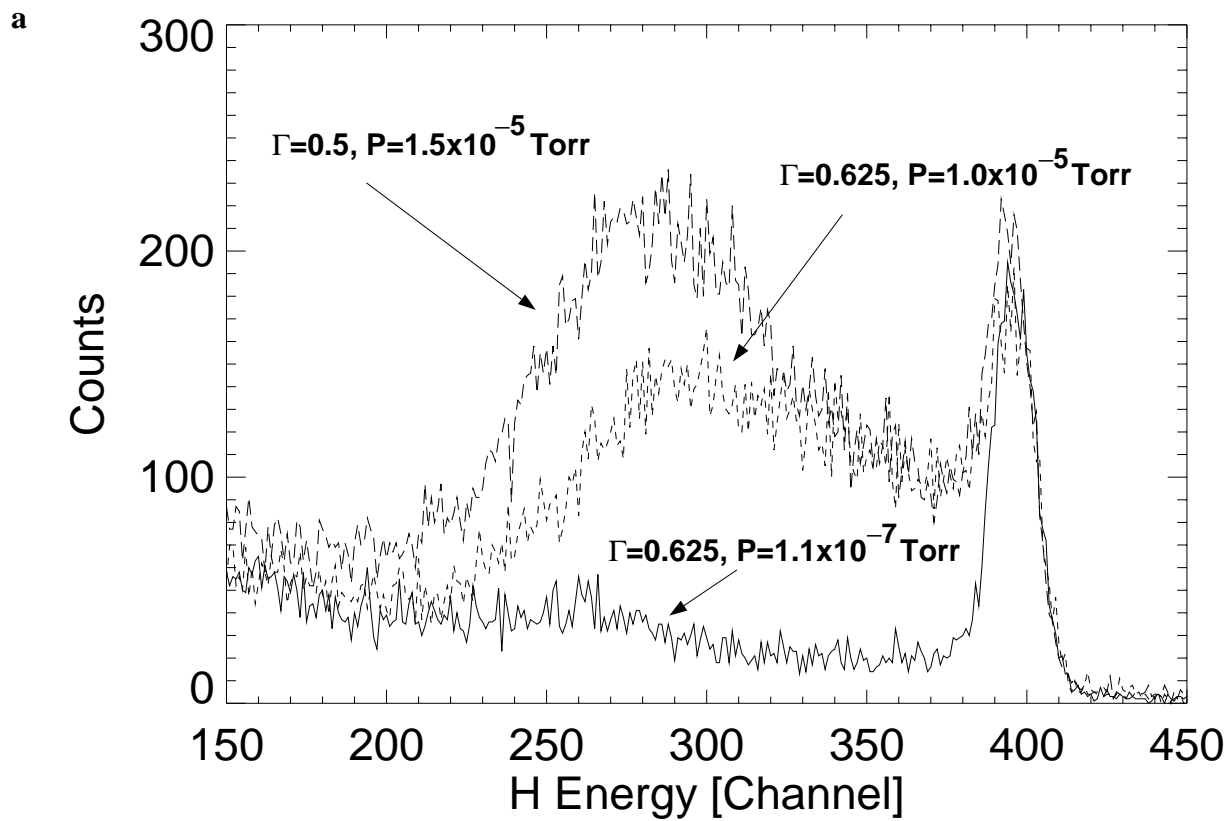


Figure 4.

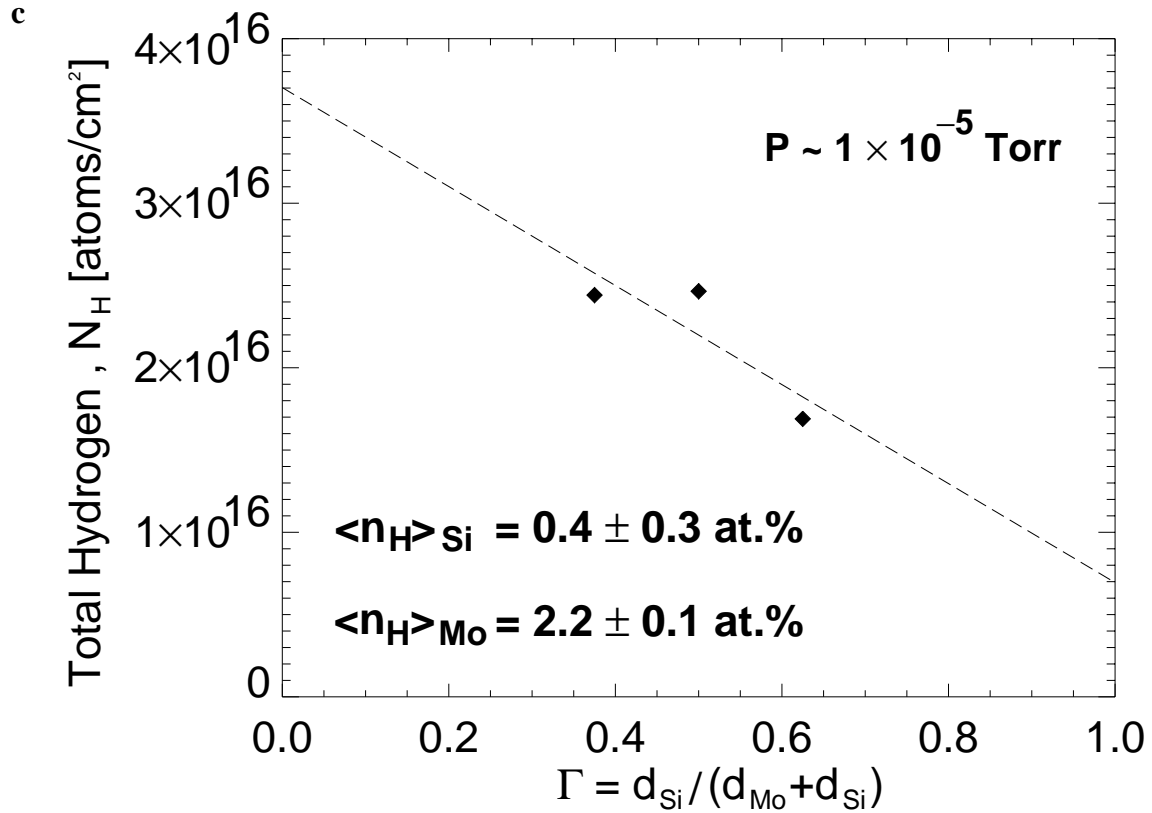
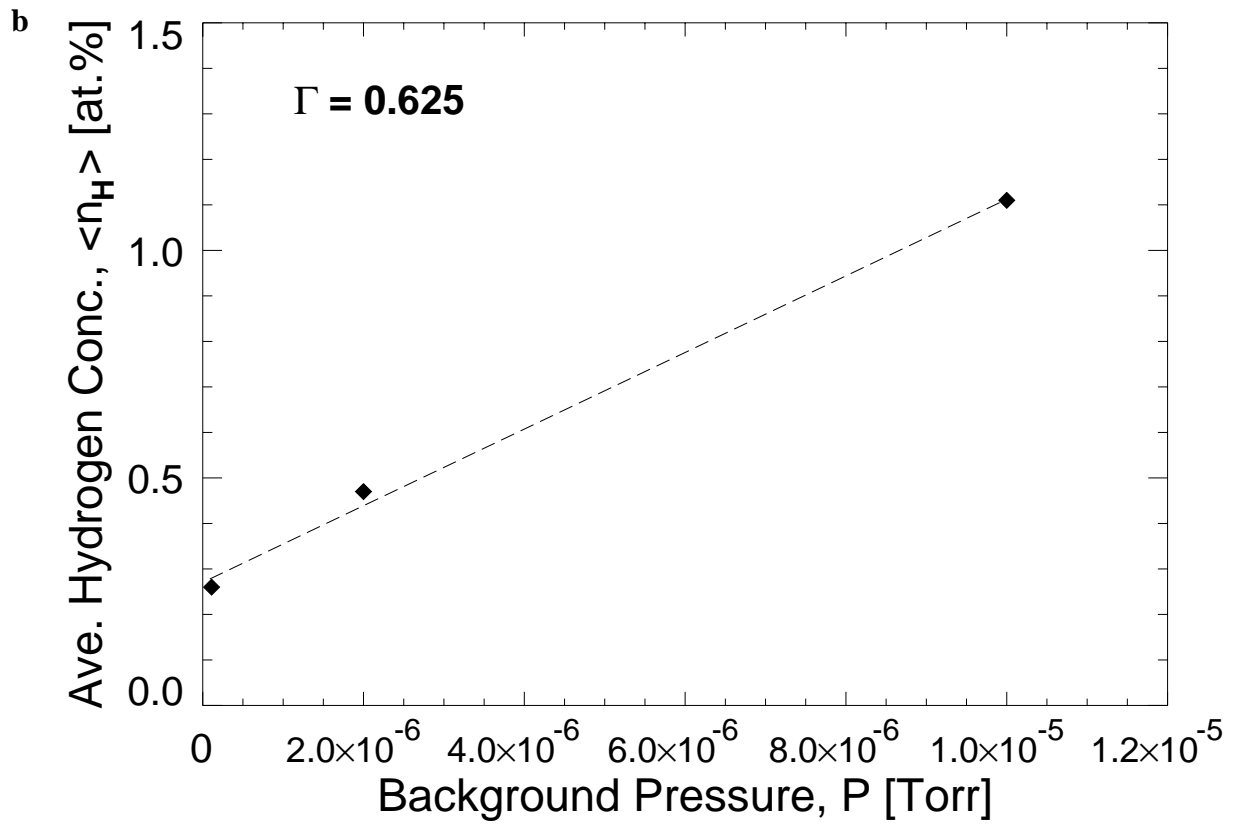


Figure 4. (cont.)